ACS APPLIED MATERIALS & INTERFACES

www.acsami.org

Research Article

Tough Thermal-Step-Responsive Shape Memory-Assisted Self-Healing Elastomers for Macroscopic Puncture Repair

Jie Zheng,[⊥] Zhongxin Ping,[⊥] Fang Xie,* Yanju Liu, and Jinsong Leng*

Cite This: *ACS Appl. Mater. Interfaces* 2026, 18, 7452−7461

Read Online

ACCESS | Metrics & More | Article Recommendations | Supporting Information

ABSTRACT: Self-healing polymers significantly extend the service life and enhance the operational reliability of devices. However, conventional self-healing polymers are often ineffective against macroscopic deformations and holes. Shape memory-assisted self-healing (SMASH) provides a feasible solution to this challenge. Efficient shape recovery relies on stable cross-links. While chemical cross-links provide a powerful driving force for shape recovery, they inherently hinder self-healing due to their irreversibility. Conversely, weak physical cross-links generally result in lower tensile strength and unsatisfactory shape recovery. Herein, metal coordination bonds are utilized as dynamic cross-links to construct tough thermal-step-responsive SMASH polyurethanes. Strong Zn^{2+}-pyridine coordination bonds endow the elastomers with the ability to repair macroscopic punctures. Without external load intervention, centimeter-sized punctures (d = 1.4 cm) in such elastomers can autonomously close within 1 min at 40 °C, followed by complete healing at 70 °C to repair macroscopic damage. These coordination bonds serve as dynamic cross-links to significantly enhance mechanical properties (49.71 MPa for strength and 138.17 MJ/m^3 for toughness). The coordination cross-links play three key roles in the repair process: (1) during the damage process, they act as network anchors to ensure maximum storage of entropic energy within the polymer network; (2) during hole closure, they facilitate efficient release of this stored energy to provide the recovery driving force; and (3) during the healing stage, their reversible dissociation releases polymer chains, which accelerates dynamic bond exchange at the damaged interfaces. This study provides valuable insights into developing tough self-healing soft materials for macroscopic damage repair.

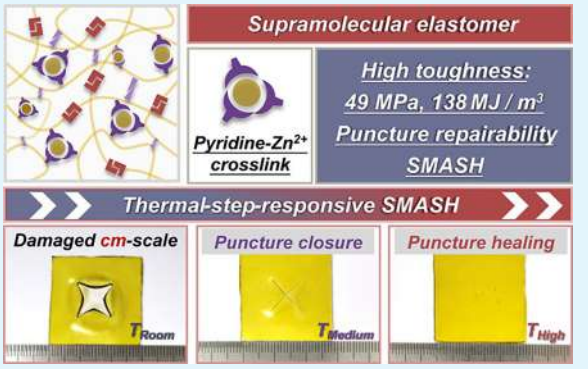

KEYWORDS: *metal coordination bond, self-healing, macroscopic damage, shape memory polymer, toughness*

1. INTRODUCTION

To ensure the long-term stable operation of flexible devices, the constituent elastomers must be capable of withstanding repeated deformation and rapidly recovering their electrical conductivity and mechanical properties after damage.[1,2] Self-healing elastomers can autonomously restore their structure integrity and functionality following external damage, thereby significantly extending service life and reliability while reducing maintenance costs.[3−5] Consequently, these materials hold immense potential for applications in flexible electronic devices, biomedical implants, and high-sensitivity sensor systems.[6−9] However, conventional self-healing polymers rely primarily on molecular chain diffusion and dynamic bond rearrangement.[10] When facing macroscopic damage such as punctures or tears, these materials often exhibit limited repair efficiency or fail completely due to the lack of sufficient driving force to close the gap.[11]

Under normal conditions, thermoplastic elastomers typically require contact between damaged interfaces to initiate self-healing via physical diffusion or chemical bond exchange.[12] However, puncture damage often causes macroscopic deformation and creates physical voids, separating the interfaces and rendering conventional healing mechanisms ineffective.[13] To address this challenge, various strategies have been proposed to facilitate the repair of macroscopic damage.[14−17] For instance, Thomas et al. reported a highly efficient kinetic energy-absorbing rigid polymer based on a Diels−Alder covalent adaptive network.[18] This polymer can close perforations through entropic elastic contraction under supersonic impact to initiate repair. However, this mechanism relies on extreme dynamic loading, making it unsuitable for common quasi-static damage scenarios. Cooper et al. utilized interfacial tension between incompatible polymers to achieve autonomous alignment in multilayer soft materials.[19] However, this method is limited to interlayer misalignment and fails

Received: December 2, 2025
Revised: January 12, 2026
Accepted: January 16, 2026
Published: January 22, 2026

https://doi.org/10.1021/acsami.5c24286
ACS Appl. Mater. Interfaces 2026, 18, 7452−7461

Scheme 1. (a) Schematic of Conventional Shape Memory-Assisted Self-Healing Mechanisms; (b) Mechanism of Thermal-Step-Responsive Shape Memory-Assisted Self-Healing Based on Metal Coordination Cross-linking

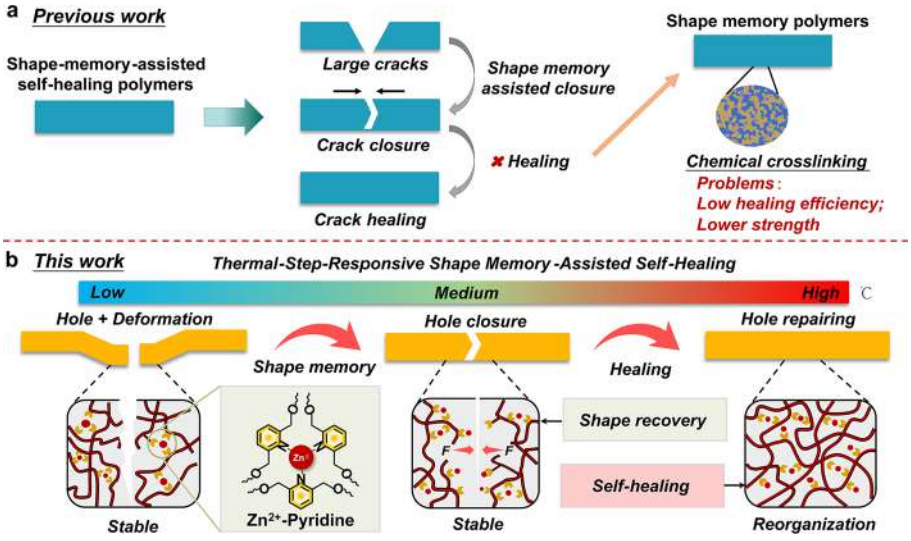

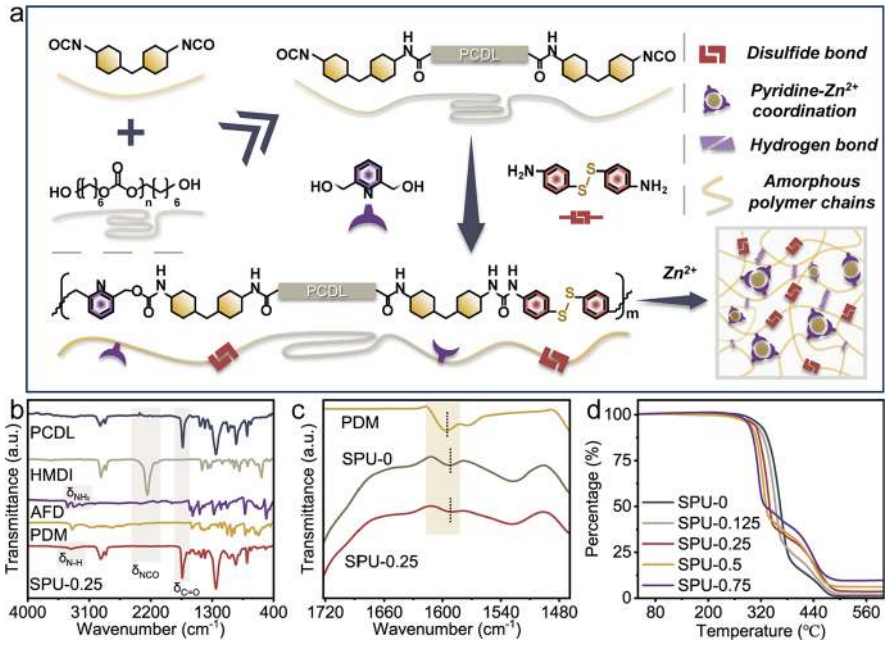

Figure 1. Synthesis route and characterization of SPU-X elastomers. (a) Schematic illustrating the synthesis of SPU-X elastomers. (b, c) FTIR spectra and (d) thermogravimetry curves of SPU-X elastomers.

when severe deformation prevents the layers from returning to their initial contact state. In contrast, shape memory polymers (SMPs) can recover their original shape upon stimulation, offering a viable mechanism to physically close macroscopic cracks.[20] Combining shape memory effects with intrinsic self-healing capabilities (i.e., shape memory-assisted self-healing [SMASH][21]) has proven effective in closing both minor scratches and macroscopic cracks (Scheme 1a).[22] Nevertheless, the inherently low energy density of most SMPs restricts their actuation capacity, often limiting repair to microscopic defects rather than macroscopic voids.[23] To overcome this, significant efforts have been directed toward engineering polymer networks with enhanced actuation capabilities. Notably, Wang et al. reported a dynamic covalent SMP network that mimics biological muscles, exhibiting high specific energy density and strong actuation force.[24] Recently, Bao et al. developed high-energy-density shape-memory rigid polymers based on strain-induced supramolecular nanostructures, achieving the first successful closure and repair of centimeter-scale punctures.[25] While these pioneering studies have significantly advanced the field, most focused on rigid polymers. Translating these strategies to shape-memory-assisted self-healing elastomers remains challenging, thereby limiting their applicability in flexible electronics and biomedicine. SMPs require a stable cross-linked network to memorize and restore the permanent shape.[26] While chemical cross-linking provides the necessary restorative force, it inherently restricts polymer chain mobility, thereby impairing self-healing efficiency.[27] Conversely, weak physical cross-links enhance dynamic properties but often fail to provide sufficient driving force for shape recovery.[28] Metal coordination bonds represent a unique class of supramolecular interactions,

https://doi.org/10.1021/acsami.5c24286
ACS Appl. Mater. Interfaces 2026, 18, 7452−7461

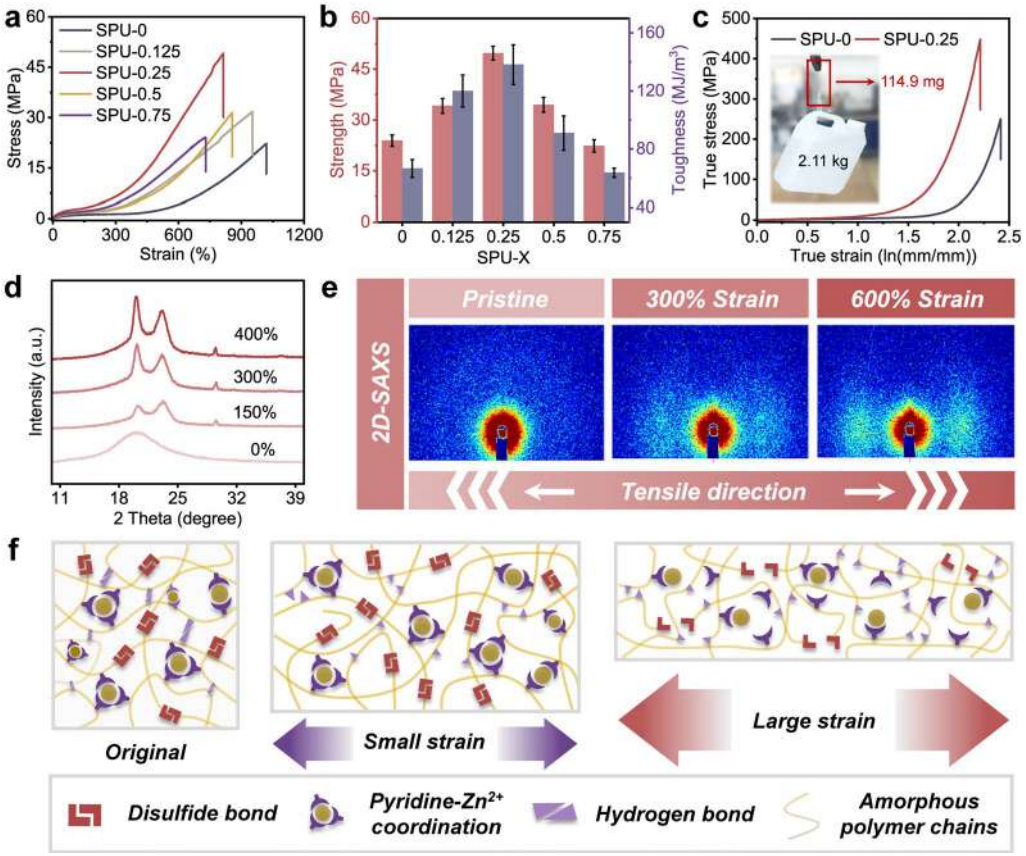

Figure 2. Mechanical properties and toughening of SPU-X. (a) Engineering stress−strain curves of SPU-X. (b) Strength and toughness comparison of SPU-X. Error bars represent standard deviation (n = 3). (c) True stress−strain curves of SPU-X. (d) WAXD and (e) 2D-SAXS patterns of SPU-0.25 at different strains. (f) Schematic of the mechanism of enhanced mechanical properties of SPU-0.25 with Zn^{2+}-pyridine cross-linking.

exhibiting both significant thermal reversibility and bond strengths comparable to covalent bonds.[29] This unique combination makes them an ideal platform for constructing materials that balance structural stability with efficient self-healing. Therefore, developing tough thermoplastic elastomers capable of repairing macroscopic puncture damage remains a critical challenge and is the core objective of this study.

Given the inherent contradiction between the stable cross-linked network required for shape memory effect and the dynamic reversible bonding required for efficient self-healing, existing shape memory-assisted self-healing (SMASH) elastomers often fail to repair macroscopic puncture injuries. Herein, this work proposes to use Zn^{2+}-pyridine coordination with appropriate strength as dynamic cross-links to endow elastomers with thermally responsive shape memory-assisted self-healing, thereby realizing macroscopic damage repair. As illustrated in Scheme 1b, these coordination bonds function as strong physical network anchors at room temperature, providing the necessary driving force for shape recovery. Conversely, at elevated temperatures, the dynamic thermal reversibility of these bonds triggers their dissociation, releasing tethered polymer chains to activate the self-healing process. A key advantage of this strategy is the precise sequential decoupling of shape memory and self-healing: during heating, the material first utilizes the stable network to achieve macroscopic crack closure before activating molecular diffusion for microscopic healing. This mechanism effectively circumvents shape recovery failure caused by premature interfacial adhesion, ultimately enabling the complete repair of centimeter-scale punctures. These coordination bonds optimize the microphase separation structure of PU, and combined with the strain-induced crystallization effect, greatly enhance its mechanical properties (strength of 49.71 MPa and toughness of 138.17 MJ/m^3). This study not only resolves the challenge of macroscopic damage repair but also provides a new paradigm for designing robust, tough, and impact-resistant smart soft materials.

2. RESULTS AND DISCUSSION

2.1. Synthesis of Ultratough Elastomers

The SPU-X samples were prepared via a prepolymer method (Figure 1a). Polycarbonate diol (PCDL; −OH) was reacted with dicyclohexylmethane-4,4′-diisocyanate (HMDI; −NCO) for 17 h in a N_2 atmosphere at 60 °C. The resulting product was then reacted with 4-aminophenyl disulfide (AFD; $-NH_2$) and 2,6-pyridinedimethanol (PDM; −OH) for 24 h to obtain SPU-0. The SPU-0 solution was then mixed with zinc trifluoromethylsulfonate ($Zn(OTf)_2$)/pyridine solutions with different molar ratios, yielding specimens with shape memory and self-healing properties (denoted as SPU-X). Notably, the formation of metal−ligand coordination bonds between zinc ions (Zn^{2+}) and pyridine is crucial for preparing SPU elastomers with shape memory-assisted self-healing properties. Since the bond energy of coordination interactions can be tailored by manipulating the metal−ligand combination, this approach offers a versatile pathway for precisely tuning material properties. The selection of the Zn^{2+}-pyridine system is based on the following considerations: (1) As a

https://doi.org/10.1021/acsami.5c24286
ACS Appl. Mater. Interfaces 2026, 18, 7452−7461

monodentate ligand, pyridine forms coordination bonds that can reversibly dissociate and reorganize at relatively mild temperatures, thereby facilitating efficient self-healing.[29] (2) Among potential candidates, Zn^{2+} exhibits a superior binding affinity for pyridine. This ensures the coordination bonds remain robust at room temperature, significantly enhancing the mechanical strength and toughness of the elastomer.[30]

The successful synthesis of the SPU-0 matrix and the formation of Zn^{2+}-pyridine coordination complexes were confirmed by Fourier transform infrared (FTIR) spectroscopy (Figure 1b,c) and nuclear magnetic resonance (NMR) analysis (Figure S1). In the FTIR spectra, absorption peaks at 1737 and 1245 cm^{-1} were attributed to the stretching vibrations of C═O (carbonyl group) and C−O (ester group), respectively. The complete absence of the characteristic isocyanate peak at 2246 cm^{-1} indicates the quantitative conversion of the reactants.[31] Furthermore, the N−H stretching vibration peak, initially exhibiting a doublet at 3420 and 3320 cm^{-1} (characteristic of primary amines), evolved into a single peak at 3367 cm^{-1}. This transition confirms the transformation of primary amines into secondary amines and the successful formation of urea groups. Crucially, the characteristic peak of the pyridine ring shifted from 1595 to 1593 cm^{-1} following the reaction, with a marked reduction in intensity upon the introduction of Zn^{2+}. This spectral shift is consistent with the electronic rearrangement induced by metal−ligand coordination interactions, verifying the formation of coordination bonds between Zn^{2+} and the pyridine nitrogen atom.[32] Complementarily, the ^1H NMR spectrum of SPU-0.25 clearly displays the characteristic signals of the pyridine ring and disulfide linkages, confirming the successful covalent incorporation of the chain extender into the polyurethane backbone. To further elucidate the thermal-step-responsive mechanism at the molecular level, variable-temperature FTIR (VT-FTIR) spectra were recorded (Figure S3). Upon heating from room temperature to 100 °C, the pyridine characteristic peak (~1590 cm^{-1}) displayed a gradual blue shift accompanied by a significant increase in intensity. This evolution provides direct evidence for the progressive dissociation of the Zn^{2+}-pyridine coordination bonds and the liberation of free pyridine moieties. The thermal unlocking of these physical cross-links imparts high mobility to the polymer chains, which is a prerequisite for the efficient self-healing capability observed in this system.

The thermal stability of the SPU-X series was systematically investigated via thermogravimetric analysis (TGA) (Figure 1d). All polymers exhibited near-complete decomposition by 600 °C. Notably, the residual mass gradually increased from 1.31 to 9.72%, with the incorporation of Zn^{2+} (that is, $Zn(OTf)_2$), directly correlating with the increasing content of nonvolatile zinc species. Despite the increase in residue, the introduction of Zn^{2+} resulted in a slight compromise in thermal stability. Specifically, the initial decomposition temperature of the SPU-X samples decreased by approximately 11−23 °C compared to the pristine SPU-0. This reduction is attributed to the formation of a Zn^{2+}-pyridine coordination network, which strongly promotes the aggregation of hard segments. The intensified microphase separation amplifies the thermodynamic incompatibility between the soft and hard phases. Consequently, these unstable phase interfaces likely act as initiation sites for thermal degradation at lower temperatures.[33]

2.2. Toughening Effect and Mechanism

Uniaxial tensile testing was conducted to investigate the mechanical properties of SPU-X under a stretching rate of 30 mm/min at room temperature (Figure 2a,b). The pristine SPU-0 lacked coordination cross-links and consequently exhibited the lowest mechanical performance. It recorded a tensile strength of 24.65 MPa, an elongation at break of 989%, and a toughness of 68.2 MJ/m^3. Upon the introduction of Zn^{2+}, the mechanical properties significantly improved, displaying a trend of initially increasing and then decreasing with rising zinc content. Notably, the optimal sample, SPU-0.25, achieved a tensile strength of 49.71 MPa and a toughness of 138.17 MJ/m^3. These values represent a ~2-fold increase compared to those of SPU-0. Complementing the engineering stress−strain data, the true stress−strain curves (Figure 2c) reveal that SPU-0.25 reached a remarkable true stress of 462.31 MPa, significantly surpassing the 268.44 MPa of SPU-0. To visually demonstrate this strength, a thin SPU-0.25 film (0.114 g) successfully withstood a load of 2.11 kg (18,509 times the sample weight; Figure 2c inset). Furthermore, the SPU-0.25 exhibited superior comprehensive mechanical properties compared to many previously reported analogues (Figure S2). Tensile test results indicate that Zn^{2+}-pyridine bonds play a crucial role in enhancing the mechanical properties of materials. This performance enhancement is primarily attributed to a sacrificial bond mechanism based on dynamic Zn^{2+}-pyridine coordination cross-links.[34] However, mechanical performance deteriorates when the Zn^{2+} to pyridine ratio exceeds 0.5. This decline stems from an excessive cross-link density.[35] Such high density promotes the aggregation of rigid segments into larger domains. Consequently, these large aggregates act as stress concentration sites, leading to premature material failure.[36]

Subsequently, phase separation in SPU films was investigated to determine the impact of coordination cross-linking on the polymer structure. Atomic force microscopy (AFM) images (Figure S4) reveal the distinct aggregation of hard (bright) and soft (dark) segments, confirming a microphase-separated structure. Optimal microphase separation is known to enhance elastomer mechanics. Conversely, excessive phase separation leads to severe hard segment aggregation, inducing stress concentration that deteriorates material performance.[37] The phase image of pristine SPU-0 displays a relatively homogeneous morphology with negligible microphase separation. Introducing a small amount of Zn^{2+} (SPU-0.125) initiates localized hard segment aggregation driven by coordination bond formation. Notably, SPU-0.25 exhibits the most well-defined and uniform microphase-separated morphology. In this state, finely dispersed nanoscale hard domains facilitate effective stress transfer. This structure correlates with the optimal mechanical performance observed. However, further increasing Zn^{2+} content intensifies phase separation, leading to domain coarsening and severe aggregation. These large rigid domains act as stress concentration sites and compromise mechanical strength. Having identified SPU-0.25 as the optimal formulation, we used in situ variable-temperature AFM (Figure S5) to visually corroborate the thermal-step-responsive mechanism. From room temperature to 60 °C, the material retains a well-defined skeleton with minor boundary blurring due to thermal motion. This stability confirms that the Zn^{2+}-pyridine coordination network remains intact. These physical cross-links provide the entropic elasticity required for shape recovery. Heating to 70 °C triggers a distinct transition

https://doi.org/10.1021/acsami.5c24286
ACS Appl. Mater. Interfaces 2026, 18, 7452−7461

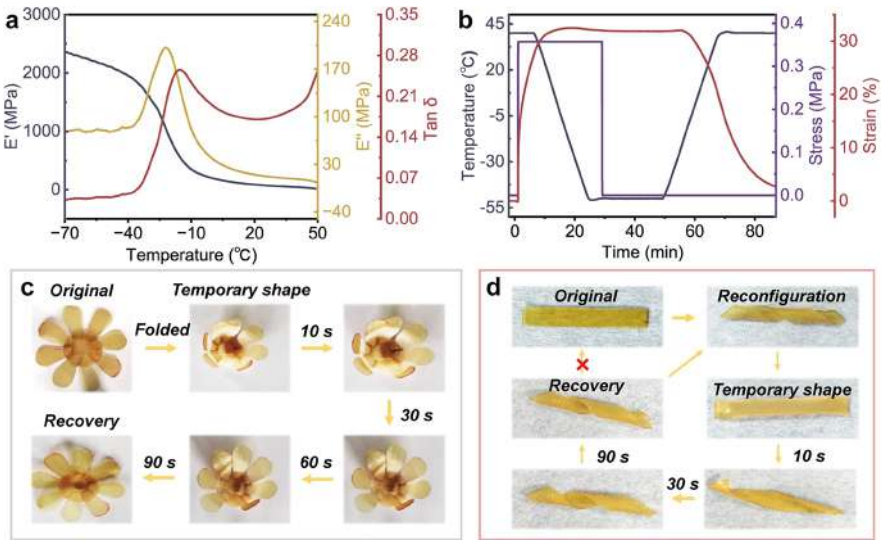

Figure 3. Shape memory and reconfiguration properties of SPU-0.25. (a) Storage modulus (E'), loss modulus (E''), and loss factor (tan δ) of the SPU-0.25 sample. (b) Shape memory cycle of SPU-0.25. (c,d) Photographs illustrating the (c) shape memory effect and (d) shape-reconstructing properties of SPU-0.25.

characterized by the emergence of large bright aggregates and blurred interfaces. This thermally induced phase coarsening results from the dynamic activation of coordination bonds and disulfide exchange. This critical state unlocks chain mobility for healing while retaining sufficient viscosity to prevent structural collapse. Heating further to 80−100 °C dissolves these aggregates into a homogenized flow state. Thus, 70 °C represents the optimal balance between mobility and integrity for efficient repair.

To further elucidate the molecular-level chain packing and aggregation structure, wide-angle X-ray diffraction (WAXD) analysis was conducted. To verify the impact of coordination bonds on crystallinity, we compared the WAXD pattern of SPU-0.25 with that of the control sample SPU-0 (Figure S6). SPU-0 exhibited distinct diffraction peaks at 2θ of 20.0° and 23.4°, corresponding to the crystalline PCDL phase. In contrast, these peaks disappeared in SPU-0.25, replaced by a broad amorphous halo. This confirms that the Zn^{2+}-pyridine cross-linking significantly restricts chain mobility. Consequently, it disrupts the structural ordering and effectively inhibits PCDL crystallization. To elucidate the mechanism governing noncovalent interactions during stretching, the materials were subjected to small-angle X-ray scattering (SAXS) and WAXD analysis at various strain levels. As shown in Figure 2d, diffraction peaks corresponding to crystalline PCDL emerge when tensile strain exceeds 150%. Their intensity increases markedly with further strain. This trend indicates that stretching induces chain alignment and ordering, leading to strain-induced crystallization (SIC). SIC acts as a critical self-reinforcing mechanism. It effectively dissipates energy and enhances mechanical toughness, aligning with recent findings in tough elastomers.[38,39] Concurrently, 2D-SAXS images reveal that the isotropic scattering pattern transforms from circular to rhomboidal (Figure 2e). This shape change suggests that the phase separation domains deform significantly at 300% strain. At 600% strain, the scattering intensity increases sharply. At this stage, the rapid disruption of coordination and hydrogen bonds triggers the collapse of the phase-separated domains. This collapse enables the elastomer chains to orient highly along the stretching direction.

The structure−property relationship of SPU-0.25 can be summarized based on the experimental results (Figure 2f). AFM analysis confirms that the elastomer possesses a distinct microphase-separated structure. Within this framework, the Zn^{2+}-pyridine coordination bonds play a crucial dual role depending on the external environment. At ambient temperature, they serve as stable physical cross-links within hard domains, effectively restricting chain slippage to ensure high mechanical strength. Under strain, these bonds act as sacrificial units. Their dissociation dissipates energy and facilitates the alignment of soft segments.[40] This alignment subsequently induces strain-induced crystallization (SIC), which acts as a self-reinforcing mechanism to enhance toughness.[41] Conversely, heating activates the dynamic reversibility of the coordination motifs. Their rapid dissociation temporarily disassembles the physical network, unlocking polymer chains from their restricted state. The resulting high mobility facilitates molecular diffusion across interfaces, thereby enabling efficient self-healing.

2.3. Thermo-Mechanical and Shape-Memory Properties

Dynamic mechanical analysis (DMA) was performed to determine the storage modulus (E'), loss modulus (E''), and loss factor (tan δ) of the SPU-0.25 specimens (Figure 3a). The storage modulus of the SPU-0.25 sample began to decrease from −70 °C and dropped sharply from approximately 1300 to 400 MPa near −16 °C. Furthermore, differential scanning calorimetry (DSC) measurements estimated the glass transition temperature (T_g) of all Zn^{2+}-incorporated SPU samples to be approximately −30 °C (Figure S7). Based on these results, an appropriate temperature protocol was selected for the shape memory tests on the SPU-0.25 sample, which were conducted by DMA. For instance, the sample was heated to 40 °C and equilibrated, followed by the application of a 2 N tensile load maintained for 5 min (Figure 3b). The sample was then cooled below T_g for 20 min. As the molecular chain motion was frozen, the deformation was fixed, resulting in the intended temporary shape. The shape fixity ratio (R_f) was calculated to be 98.07%. Upon reheating to 40 °C, the sample recovered its original shape, with a shape recovery ratio (R_r) of

https://doi.org/10.1021/acsami.5c24286
ACS Appl. Mater. Interfaces 2026, 18, 7452−7461

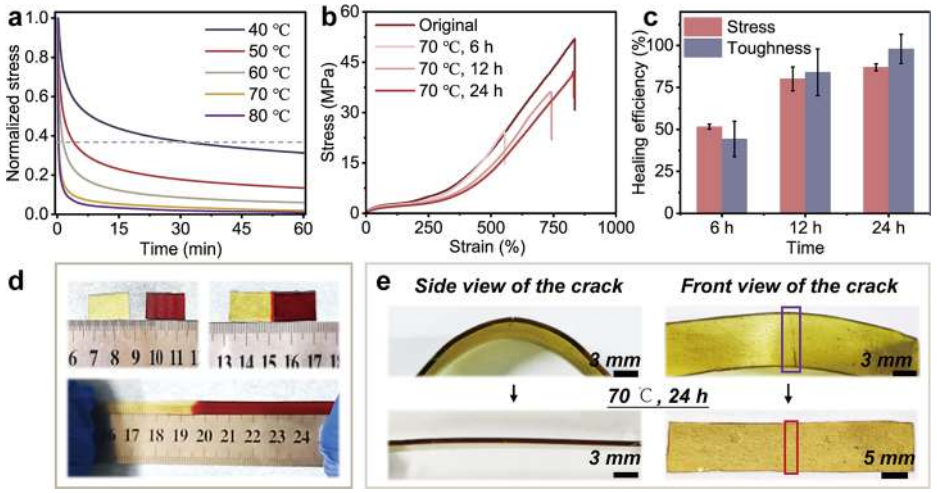

Figure 4. Self-healing properties of SPU-0.25. (a) Stress relaxation curves of SPU-0.25 at different temperatures. (b) Stress−strain curves of the healed SPU-0.25 samples. (c) Healing efficiency of tensile strength and toughness for SPU-0.25. Error bars represent standard deviation (n = 3). (d) Digital images of the SPU-0.25 sample before and after the self-healing process. (e) Side and front views of SPU-0.25 before and after healing.

89.21%. To demonstrate the shape memory effect of SPU-0.25 visually, the sample was cut and bent into a flower-like shape (Figure 3c). At room temperature, the petals gradually unfolded within 90 s, confirming excellent shape recovery.

Beyond shape memory, SPU-0.25 exhibits distinct shape reconfigurability enabled by dynamic supramolecular exchange. A reconfiguration temperature of 70 °C was selected to activate chain mobility and reorganization. As shown in Figure 3d, a rectangular strip was twisted into a spring shape and annealed at 70 °C for 3 h to reset the permanent shape. The new spring shape was then unfolded and temporarily fixed by cooling. Upon reheating to room temperature, the sample automatically reverted to the spring form rather than the original rectangle. This observation confirms the material's robust capability for permanent shape reconfiguration.

2.4. Self-Healing Mechanisms and Shape Memory-Assisted Self-Healing

The self-healing capability of the SPU elastomer stems from a synergistic dynamic network comprising hydrogen bonds, Zn^{2+}-pyridine coordination interactions, and disulfide linkages. Since the healing efficiency is intrinsically governed by the mobility of molecular chains, stress relaxation analysis was employed to probe the dissociation kinetics and topological rearrangement of these dynamic bonds. At 40 °C, the material exhibited a prolonged relaxation time (Figure 4a), confirming that the dynamic motifs function as stable physical cross-links that effectively restrict chain slippage. Conversely, the relaxation rate accelerated markedly with increasing temperature. Notably, at 60 °C, the relaxation time decreased to 1.49 min. Upon heating to 70 °C, the relaxation rate reached its maximum. Further temperature increases had no significant effect. This distinct transition signifies the full activation of bond exchange reactions for the Zn^{2+}-pyridine and disulfide moieties. This activation liberates the polymer chains, providing the requisite mobility for interfacial reconstruction and healing. Quantitatively, the activation energy for the stress relaxation process was calculated as 124 kJ/mol from the Arrhenius fitting (Figure S9). This calculation indicates the material's high sensitivity to temperature fluctuations, which is a hallmark of dynamic bond exchange reactions.[42] The material's sensitivity to temperature enables its dimensional stability and mechanical strength to be maintained at room temperature while facilitating efficient self-healing at elevated temperatures.

To comprehensively assess repairability, we evaluated the recovery of both tensile strength and toughness for SPU-0.25 (Figure 4b,c). Guided by the stress relaxation results, 70 °C was selected as the healing temperature to ensure sufficient chain mobility. The quantitative results demonstrate that healing efficiency improves significantly with time. After 6 h, the sample recovered 51.64% of its tensile strength and 15.36% of its toughness. Extending the healing duration to 24 h markedly improved these values to 86.96 and 81.61%, respectively. This recovery is driven by thermal stimulation. The elevated temperature provides kinetic energy for segment rearrangement and interdiffusion. Consequently, this facilitates the dynamic reconstruction of the physical network across the fractured interface.

Macroscopic self-healing was visually evaluated. To verify the mechanism of molecular interdiffusion, we first conducted a cutting-rejoining experiment using a Sudan Red-dyed sample (Figure 4d). After healing, a clear color gradient emerged at the interface, and the healed sample could be stretched without breaking. This confirms that thermal activation drives effective polymer chain diffusion and re-entanglement across the damage zone. Subsequently, a deep incision test was performed (Figure 4e). A deep cut was made on the SPU film. After heating at 70 °C for 24 h, the incision healed completely, resulting in a smooth surface with no visible scars from either the side or front view. Moreover, the absence of permanent covalent cross-links endows the SPU elastomers with excellent recyclability. As shown in Figure S10, all SPU samples dissolved completely in *N*,*N*-dimethylformamide (DMF). This capability facilitates efficient recovery and reprocessing via solution casting, aligning with recent strategies for sustainable elastomers.[43]

Thermal-step-responsive shape memory-assisted self-healing. Wool and O'Connor[44] proposed a theory of crack healing in polymers comprising five stages: (a) surface rearrangement; (b) surface approach; (c) wetting; (d) diffusion; and (e) randomization. Fundamentally, physical contact between fractured surfaces is the prerequisite for molecular diffusion, bond exchange, and property recovery. In our design, the

https://doi.org/10.1021/acsami.5c24286
ACS Appl. Mater. Interfaces 2026, 18, 7452−7461

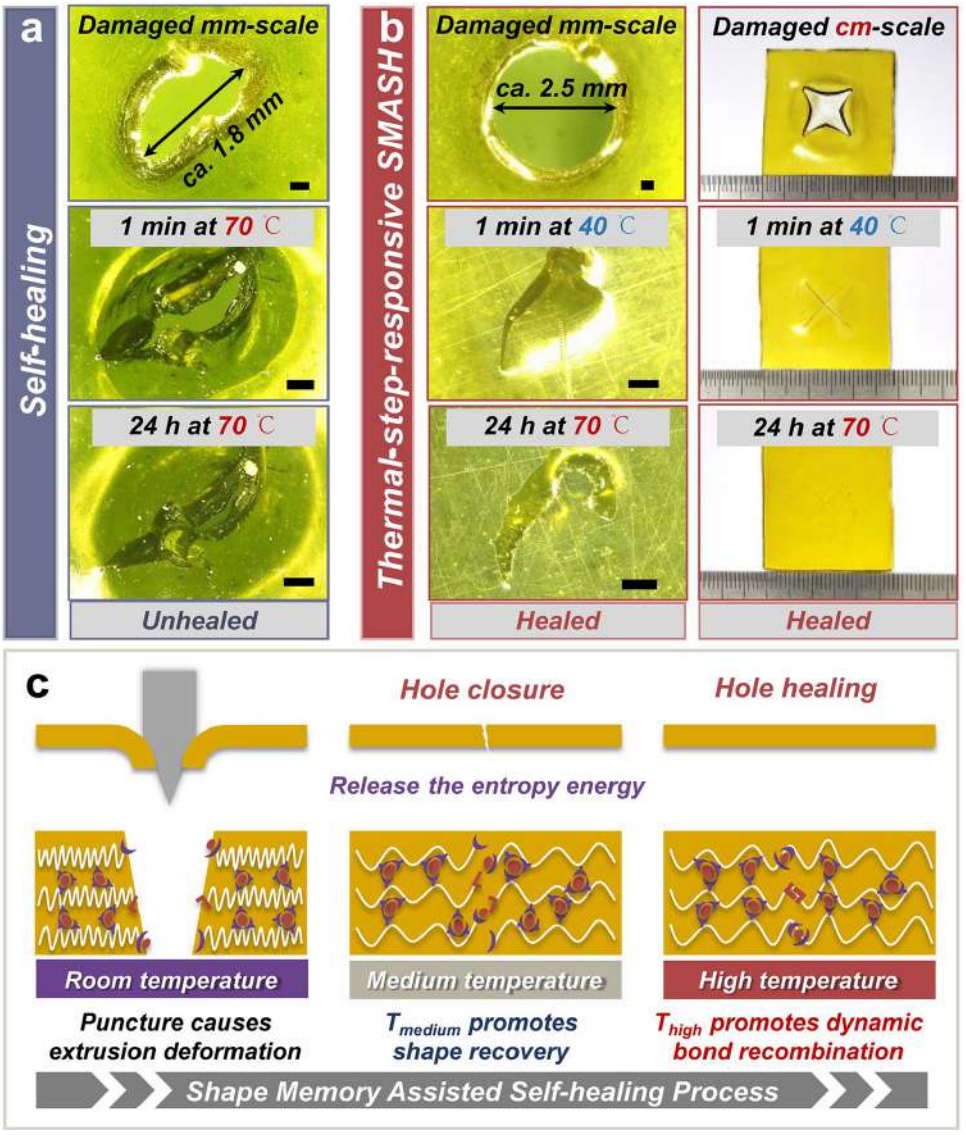

Figure 5. Shape memory-assisted self-healing (SMASH) properties of SPU-0.25. (a) Image of a punctured SPU-0.25 film with a 1.8 mm-diameter hole after damage (top), after 1 min of heating at 70 °C oven (center), and after 24 h at 70 °C (bottom). Scale bar represents 250 μm. (b) Image of a punctured SPU-0.25 film with a 2.5 mm-diameter hole and a 1.4 cm-diameter hole after damage (top), after 1 min of heating at 40 °C oven (center), and after 24 h at 70 °C (bottom). (c) Schematic illustration of the thermal-step-responsive SMASH mechanism.

shape memory and self-healing processes are orchestrated into distinct thermal stages to achieve synergistic functionality. This strategy ensures that the macroscopic crack is physically closed via the shape memory effect before the activation of molecular-level healing. Crucially, the Zn^{2+}-pyridine coordination bonds fulfill a dual role governed by temperature. During the shape memory stage (Step 1), these bonds act as stable cross-links, driving the elastic recovery to close the puncture. Upon further heating to the healing stage (Step 2), they reversibly dissociate. This dissociation significantly enhances chain mobility, facilitating the diffusion and recombination across the closed interface.

To validate this mechanism, we experimentally investigated the thermal-step-responsive behavior of SPU-0.25. A film was punctured using a sharp iron rod (Figure S11). In a control experiment, the damaged sample was heated directly to 70 °C (Figures 5a and S13). Under this condition, the simultaneous requirement for stable cross-links (for shape recovery) and chain mobility (for healing) created a structural conflict, resulting in incomplete repair. Conversely, our designed phased protocol—heating at 40 °C to trigger shape recovery followed by 70 °C for healing—achieved excellent functional synergy, successfully repairing the puncture (Figures 5b and S14). To demonstrate robustness, we further expanded the damage diameter to 1.4 cm (centimeter-scale) and achieved full healing. Additionally, we found that samples without added Zn^{2+} exhibit very weak self-healing capabilities (Figures S15 and S16). To probe the underlying mechanism, the cyclic shape memory performance of SPU-0 was evaluated (Figure S17). Compared to the Zn^{2+}-coordinated SPUs, SPU-0 exhibited a lower fixity ratio (R_f = 92.89%) and a significantly reduced recovery ratio (R_r = 82.43%). This quantitative evidence confirms that without the Zn^{2+}-pyridine coordination acting as stable physical cross-links, the polymer chains cannot effectively store the entropic energy during deformation. Consequently, the material lacks sufficient recovery driving force to close the macroscopic puncture, leading to the observed poor healing performance. These experiments verify

https://doi.org/10.1021/acsami.5c24286
ACS Appl. Mater. Interfaces 2026, 18, 7452−7461

that the SPU-0.25 sample exhibits sequential shape memory and self-healing behavior under thermal induction, demonstrating distinct smart thermal-step-responsive characteristics (Figure 5c). Furthermore, this confirms the applicability of the thermal-step-responsive SMASH strategy for repairing extensive damage. Finally, we characterized the shape memory properties of the healed SPU-0.25 sample (Figure S19). The shape fixity ratio (R_f) and recovery ratio (R_r) reached 98.7 and 96.1%, respectively. Remarkably, these values represent an improvement over the original performance. This enhancement is likely attributed to the rearrangement of molecular chains during the healing process. This thermal annealing promotes the formation of a more homogeneous and defect-free cross-linked network structure.[45] In summary, SPU-0.25 has the potential to restore its structure and functionality via the thermal-step-responsive SMASH mechanism, even in the presence of centimeter-scale cracks. These findings offer significant implications for the design of next-generation thermoplastic elastomers combining shape memory and self-healing capabilities.

3. CONCLUSIONS

In this study, we developed tough, thermal-step-responsive SMASH elastomers capable of repairing macroscopic punctures. The core design strategy involves incorporating robust yet thermally labile metal-coordination cross-links into the polymer network. These cross-links not only enhance mechanical properties but also orchestrate the thermal-step-responsive SMASH behavior. Crucially, the temperature-dependent dynamics of the coordination bonds effectively decouple the shape memory effect from the self-healing process. Upon puncture, the stable coordination cross-links serve as network anchors. They convert the mechanical work of deformation into entropic energy stored within the network. Subsequently, at temperatures below the bond dissociation threshold, this stored energy drives shape recovery to physically close the crack. Further heating above the dissociation temperature triggers the breakage of metal-coordination bonds. This unlocks polymer chains for dynamic diffusion and bond exchange, completing the healing process. This mechanism successfully overcomes the challenge of repairing macroscopic defects. Leveraging this strategy, SPU-0.25 films achieved the repair of centimeter-scale perforations. Consequently, this work paves the way for the application of mechanically robust, self-healing soft materials in next-generation wearable electronics and biomedical devices.

4. EXPERIMENTAL SECTION

Materials

Polycarbonate diol (PCDL, M_n = 2000 g/mol) was purchased from Jining Hongming Chemical Reagent Co., Ltd. (China). Dibutyltin dilaurate, 4-aminophenyl disulfide (AFD), dicyclohexylmethane-4,4′-diisocyanate (HMDI), and *N*,*N*-dimethylformamide (DMF) were obtained from Shanghai Aladdin Biochemical Technology Co., Ltd. (China). Zinc trifluoromethanesulfonate ($Zn(OTf)_2$) and 2,6-pyridinedimethanol were supplied by Shanghai Macklin Biochemical Technology Co., Ltd. (China).

Synthesis of SPU Elastomers

The synthesis procedure for SPU-0.25 is described as follows. PCDL (M_n = 2000 g/mol, 16 g, 8 mmol) was placed in a three-necked flask and dried under vacuum at 120 °C for 3 h. The flask was then transferred to an oil bath. DMF (30 mL) was added, and the mixture was heated to 60 °C with stirring to achieve dissolution. A solution of HMDI (4.2 g, 16 mmol) in DMF (30 mL) was added dropwise to the flask. The reaction proceeded under a nitrogen atmosphere for 1 h, followed by the addition of DBTDL (55 mg, 0.087 mmol). The reaction was continued for an additional 16 h. Subsequently, PDM (0.55 g, 4 mmol) and AFD (0.99 g, 4 mmol) were added, and the reaction was allowed to proceed for 24 h. Finally, $Zn(OTf)_2$ (0.36 g, 1 mmol) was added, and the reaction continued for 3 h. The resulting viscous mixture was poured into a mold, degassed under vacuum to remove bubbles, and then cured at 70 °C for 24 h.

Characterizations

Fourier transform infrared (FTIR) spectra of SPU-X and its precursors were acquired in attenuated total reflection (ATR) mode at room temperature over the range of 400−4000 cm^{-1} using a TENSOR spectrometer (Bruker, Germany). The thermal stability of SPU-X was evaluated by thermogravimetric analysis (TGA) on an FTA449F5 instrument (Netzsch, Germany), with all measurements conducted under a nitrogen atmosphere while heating from room temperature to 600 °C at a rate of 10 °C/min. Mechanical properties of SPU-X were analyzed using a universal electronic tensile testing machine, where specimens cut into rectangular strips (60 × 10 × 0.5 mm^3) were tested at room temperature with a tensile rate of 30 mm/min. XRD data were collected using a DX-2700X diffractometer (Dandong Haoyuan, China) scanning from 5° to 90° (2θ). Thermomechanical properties were characterized using a DMA Q800 instrument (TA Instruments) in tension mode; specimens were cut into rectangular strips and tested under a constant force of 1 N at 1 Hz frequency while ramping temperature from −80 to 50 °C at 3 K/min. A stress relaxation experiment was conducted for 60 min at a constant temperature with a strain amplitude of 50%. SAXS patterns were acquired using an Anton Paar SAXSpoint 2.0 device equipped with a multilayer focused Cu Kα X-ray source (λ = 0.154 nm). In situ FT-IR measurements were conducted using the Bruker INVENIO R FT-IR spectrometer equipped with an in situ diffuse reflectance cell (Harrick). ^{1}H NMR spectra were recorded using an AVANCE NEO 400 M spectrometer. Atomic force microscopy (AFM) and in situ variable-temperature AFM measurements were carried out using a Bruker Dimension Icon scanning probe microscope.

Shape-memory tests. The shape-memory properties of SPU-X were scrutinized by DMA (TA Q800). Each sample was cut into rectangles (20 × 5 × 0.5−0.6 mm^3) and heated at 40 °C. The sample was subjected to an original strain (denoted as ε_1) and then stretched and maintained for 5 min. After noting the resulting length (denoted as ε_2), the sample was cooled to −50 °C and maintained for 5 min. Subsequently, a temporary shape (ε_3) was obtained after the force was removed. ε_4 was determined after heating the sample to 40 °C and maintaining it for 15 min.

$$R_f = \frac{\varepsilon_3 - \varepsilon_1}{\varepsilon_2 - \varepsilon_1} \times 100\% \quad (1)$$

$$R_r = \frac{\varepsilon_3 - \varepsilon_4}{\varepsilon_3 - \varepsilon_1} \times 100\% \quad (2)$$

Self-healing tests. The ability of the synthesized materials to crack and heal was probed under different conditions. The tensile strengths of the cracked and healed samples (σ_0 and σ, respectively) were used to calculate the healing efficiency (η) as follow:

$$\eta = \frac{\sigma}{\sigma_0} \times 100\% \quad (3)$$

Shape memory-assisted self-healing experiment. To verify the effectiveness of the material in repairing macroscopic cracks, a sharp tool was used to puncture the specimen and create a macroscopic hole. Then, the specimen was left at room temperature for over 15 min to fix temporary shape. Then, the specimen was placed in an oven at 40 °C. This allowed the specimen's shape to fully recover. In the final stage, the specimen was placed in an oven at 70 °C for 24 h.

https://doi.org/10.1021/acsami.5c24286
ACS Appl. Mater. Interfaces 2026, 18, 7452−7461

■ ASSOCIATED CONTENT

Supporting Information

The Supporting Information is available free of charge at https://pubs.acs.org/doi/10.1021/acsami.5c24286.

Synthesis formulations, structural and morphological characterizations (NMR, FTIR, XRD, AFM), thermal analysis, and supplementary figures regarding mechanical, self-healing, and shape-memory properties (PDF)

■ AUTHOR INFORMATION

Corresponding Authors

Fang Xie − *Department of Materials Science and Engineering, Harbin Institute of Technology at Weihai, Weihai 264209, P. R. China;* orcid.org/0000-0002-2194-0566; Email: fangxie@hit.edu.cn

Jinsong Leng − *Center for Composite Materials and Structures, Harbin Institute of Technology, Harbin 150080, P. R. China;* orcid.org/0000-0001-5098-9871; Email: lengjs@hit.edu.cn

Authors

Jie Zheng − *Center for Composite Materials and Structures, Harbin Institute of Technology, Harbin 150080, P. R. China*

Zhongxin Ping − *Center for Composite Materials and Structures, Harbin Institute of Technology, Harbin 150080, P. R. China;* orcid.org/0000-0001-5118-7985

Yanju Liu − *Department of Astronautical Science and Mechanics, Harbin Institute of Technology, Harbin 150001, P. R. China; Suzhou Research Institute, Harbin Institute of Technology, Suzhou 215104, China;* orcid.org/0000-0001-8269-1594

Complete contact information is available at: https://pubs.acs.org/10.1021/acsami.5c24286

Author Contributions

⊥J.Z. and Z.P. contributed equally to this work.

Notes

The authors declare no competing financial interest.

■ ACKNOWLEDGMENTS

This work was supported by the Natural Science Foundation of Shandong Province of China (ZR2024ME232), the National Key R&D Program of China (2022YFB3805700), and the Foundation (no. XJCL2025015) of Key Laboratory of Advanced Rubber Material, Ministry of Education.

■ REFERENCES

(1) Shi, C. Q.; Zou, Z. A.; Lei, Z. P.; Zhu, P. C.; Zhang, W.; Xiao, J. L. Heterogeneous Integration of Rigid, Soft, and Liquid Materials for Self-Healable, Recyclable, and Reconfigurable Wearable Electronics. *Sci. Adv.* **2020**, *6* (45), No. eabd0202.

(2) Wu, X.; Wang, J.; Huang, J.; Yang, S. Robust, Stretchable, and Self-Healable Supramolecular Elastomers Synergistically Cross-Linked by Hydrogen Bonds and Coordination Bonds. *ACS Appl. Mater. Interfaces* **2019**, *11* (7), 7387−7396.

(3) Utrera-Barrios, S.; Verdejo, R.; Lopez-Manchado, M. A.; Hernandez Santana, M. Evolution of Self-Healing Elastomers, from Extrinsic to Combined Intrinsic Mechanisms: A Review. *Mater. Horiz.* **2020**, *7* (11), 2882−2902.

(4) Xie, P.; Wu, G.; Liu, Y.; Hu, K.; Ma, Z.; Pei, X.; Wu, Y.; Zhou, F. High-Strength, Rapid-Recovery, Solvent-Resistant, and Recyclable Fluorinated Acrylic Polyurethane with Supramolecular and Covalently Dual-Cross-Linked Networks. *ACS Appl. Polym. Mater.* **2025**, *7* (8), 5058−5069.

(5) Xie, P.; Wu, G.; Zhen, X.; Wang, G.; Meng, Y.; Hu, K.; Liu, Y.; Pei, X.; Wu, Y.; Zhou, F. Tailoring Microphase Separation via Host−Guest Stoichiometry in Supramolecular Polyurethanes for Ultra-toughening and Self-Healing. *ACS Appl. Polym. Mater.* **2025**, *7* (23), 15987−15999.

(6) Zhang, J.; Sun, F.; Xu, J.; Zhao, Z.-H.; Fu, J. Research Progress of Human Biomimetic Self-Healing Materials. *Small* **2025**, *21* (1), No. 2408199.

(7) Xu, J.; Li, Y.; Liu, T.; Wang, D.; Sun, F.; Hu, P.; Wang, L.; Chen, J.; Wang, X.; Yao, B.; Fu, J. Room-Temperature Self-Healing Soft Composite Network with Unprecedented Crack Propagation Resistance Enabled by a Supramolecular Assembled Lamellar Structure. *Adv. Mater.* **2023**, *35* (26), No. 2300937.

(8) Xie, F.; Yang, Y.; Ping, Z.; Gong, X.; Dong, Z.; Xu, W.; Yu, J.; Yao, W.; Dong, Y. Progress and Strategies in Advanced Aerospace Materials for Extreme Environments: A Review. *Acta Astronaut.* **2026**, *238*, 184−196.

(9) Vo, N. T. P.; Nam, T. U.; Jeong, M. W.; Kim, J. S.; Jung, K. H.; Lee, Y.; Ma, G.; Gu, X.; Tok, J. B.-H.; Lee, T. I.; Bao, Z.; Oh, J. Y. Autonomous Self-Healing Supramolecular Polymer Transistors for Skin Electronics. *Nat. Commun.* **2024**, *15* (1), 3433.

(10) Li, B.; Cao, P.-F.; Saito, T.; Sokolov, A. P. Intrinsically Self-Healing Polymers: From Mechanistic Insight to Current Challenges. *Chem. Rev.* **2023**, *123* (2), 701−735.

(11) Je, P. C.; Sultan, M. T.; Selvan, C. P.; Irulappasamy, S.; Mustapha, F.; Basri, A. A.; Safri, S. N. A. Manufacturing Challenges in Self-Healing Technology for Polymer Composites — a Review. *J. Mater. Res. Technol.* **2020**, *9* (4), 7370−7379.

(12) Wang, S.; Urban, M. W. Self-Healing Polymers. *Nat. Rev. Mater.* **2020**, *5* (8), 562−583.

(13) Stukalin, E. B.; Cai, L.-H.; Kumar, N. A.; Leibler, L.; Rubinstein, M. Self-Healing of Unentangled Polymer Networks with Reversible Bonds. *Macromolecules* **2013**, *46* (18), 7525−7541.

(14) Hornat, C. C.; Urban, M. W. Entropy and Interfacial Energy Driven Self-Healable Polymers. *Nat. Commun.* **2020**, *11* (1), 1028.

(15) Michal, B. T.; Jaye, C. A.; Spencer, E. J.; Rowan, S. J. Inherently Photohealable and Thermal Shape-Memory Polydisulfide Networks. *ACS Macro Lett.* **2013**, *2* (8), 694−699.

(16) Lin, T.; Tang, Z.; Guo, B. New Design Strategy for Reversible Plasticity Shape Memory Polymers with Deformable Glassy Aggregates. *ACS Appl. Mater. Interfaces* **2014**, *6* (23), 21060−21068.

(17) Kohlmeyer, R. R.; Lor, M.; Chen, J. Remote, Local, and Chemical Programming of Healable Multishape Memory Polymer Nanocomposites. *Nano Lett.* **2012**, *12* (6), 2757−2762.

(18) Sang, Z.; Eoh, H.; Xiao, K.; Kurouski, D.; Shan, W.; Hyon, J.; Sukhishvili, S. A.; Thomas, E. L. Supersonic Puncture-Healable and Impact Resistant Covalent Adaptive Networks. *Mater. Today* **2025**, *83*, 43−53.

(19) Cooper, C. B.; Root, S. E.; Michalek, L.; Wu, S.; Lai, J.-C.; Khatib, M.; Oyakhire, S. T.; Zhao, R.; Qin, J.; Bao, Z. Autonomous Alignment and Healing in Multilayer Soft Electronics Using Immiscible Dynamic Polymers. *Science* **2023**, *380* (6648), 935−941.

(20) Ping, Z.; Xie, F.; Gong, X.; Zhang, F.; Zheng, J.; Liu, Y.; Leng, J. Tailoring Photoweldable Shape Memory Polyurethane with Intrinsic Photothermal/Fluorescence via Engineering Metal-Phenolic Systems. *Adv. Funct. Mater.* **2024**, *34* (38), No. 2402592.

(21) Rodriguez, E. D.; Luo, X.; Mather, P. T. Linear/Network Poly(ε-Caprolactone) Blends Exhibiting Shape Memory Assisted Self-Healing (SMASH). *ACS Appl. Mater. Interfaces* **2011**, *3* (2), 152−161.

(22) Xu, W.; Ping, Z.; Gong, X.; Xie, F.; Liu, Y.; Leng, J. Self-Healing Polymers Coupling Shape Memory Effect. *Langmuir* **2024**, *40* (31), 15957−15968.

(23) Yang, Y.; Davydovich, D.; Hornat, C. C.; Liu, X.; Urban, M. W. Leaf-Inspired Self-Healing Polymers. *Chem.* **2018**, *4* (8), 1928−1936.

(24) Kong, Q.; Tan, Y.; Zhang, H.; Zhu, T.; Li, Y.; Xing, Y.; Wang, X. Mimosa-Inspired Body Temperature-Responsive Shape Memory

Polymer Networks: High Energy Densities and Multi-Recyclability. *Adv. Sci.* **2024**, *11* (39), No. 2407596.
(25) Shi, Y.; Cooper, C. B.; Nogusa, T.; Lai, J.-C.; Lyu, H.; Khatib, M.; Xu, C.; Michalek, L.; Bao, Z. Shape-Memory-Assisted Self-Healing of Macroscopic Punctures via High-Energy-Density Periodic Dynamic Polymers with Tunable Actuation Temperature. *Matter* **2024**, *7* (6), 2108−2124.
(26) Xia, Y.; He, Y.; Zhang, F.; Liu, Y.; Leng, J. A Review of Shape Memory Polymers and Composites: Mechanisms, Materials, and Applications. *Adv. Mater.* **2021**, *33* (6), No. 2000713.
(27) Anthamatten, M.; Roddecha, S.; Li, J. Energy Storage Capacity of Shape-Memory Polymers. *Macromolecules* **2013**, *46* (10), 4230−4234.
(28) Hornat, C. C.; Urban, M. W. Shape Memory Effects in Self-Healing Polymers. *Prog. Polym. Sci.* **2020**, *102*, No. 101208.
(29) Li, C.-H.; Zuo, J.-L. Self-Healing Polymers Based on Coordination Bonds. *Adv. Mater.* **2020**, *32* (27), No. 1903762.
(30) Xia, H.; Wang, Z.; Xie, C.; Yu, C.; Fei, G.; Wang, Z. A Facile Strategy for Self-Healing Polyurethanes Containing Multiple Metal−Ligand Bonds. *Macromol. Rapid Commun.* **2018**, *39* (6), No. 1700678.
(31) Kim, S.-M.; Jeon, H.; Shin, S.-H.; Park, S.-A.; Jegal, J.; Hwang, S. Y.; Oh, D. X.; Park, J. Superior Toughness and Fast Self-Healing at Room Temperature Engineered by Transparent Elastomers. *Adv. Mater.* **2018**, *30* (1), No. 1705145.
(32) Wang, X. Y.; Xu, J.; Zhang, Y. M.; Wang, T.; Wang, Q.; Li, S.; Yang, Z.; Zhang, X. A Stretchable, Mechanically Robust Polymer Exhibiting Shape-Memory-Assisted Self-Healing and Clustering-Triggered Emission. *Nat. Commun.* **2023**, *14* (1), 4712.
(33) Li, Y.; Guo, W.; Li, W.; Liu, X.; Zhu, H.; Zhang, J.; Liu, X.; Wei, L.; Sun, A. Tuning Hard Phase towards Synergistic Improvement of Toughness and Self-Healing Ability of Poly(Urethane Urea) by Dual Chain Extenders and Coordinative Bonds. *Chem. Eng. J.* **2020**, *393*, No. 124583.
(34) Xu, J.; Wang, X.; Zhang, X.; Zhang, Y.; Yang, Z.; Li, S.; Tao, L.; Wang, Q.; Wang, T. Room-Temperature Self-Healing Supramolecular Polyurethanes Based on the Synergistic Strengthening of Biomimetic Hierarchical Hydrogen-Bonding Interactions and Coordination Bonds. *Chem. Eng. J.* **2023**, *451*, No. 138673.
(35) Tian, Y.; Wei, Y.; Wang, M.; Wang, J.; Li, X.; Qin, X.; Zhang, L. Ultra-Stretchable, Tough, and Self-Healing Polyurethane with Tunable Microphase Separation for Flexible Wearable Electronics. *Nano Energy* **2025**, *139*, No. 110908.
(36) Li, X.; Gong, J. P. Design Principles for Strong and Tough Hydrogels. *Nat. Rev. Mater.* **2024**, *9* (6), 380−398.
(37) Zhang, M.; Wang, Y.; Yang, M.; Sun, L.; Zhao, G.; Feng, P.; Li, N.; Liu, C.; Xu, J.; Jian, X.; Chen, Y. Construction of Mechanical Robust Elastomers by Simulating the Strengthening and Healing Process of Natural Skin toward Multifunctional Electronics. *Macromolecules* **2024**, *57* (7), 3047−3057.
(38) Wang, L.; Zhang, K.; Hou, K.; Xia, Y.; Wang, X. Bridging Small Molecule Calculations and Predictable Polymer Mechanical Properties. *Nat. Commun.* **2025**, *16* (1), 6957.
(39) Zhang, X.; Wang, L.; Zhang, K.; Zhou, K.; Hou, K.; Zhao, Z.; Li, G.; Yao, Q.; Sun, N.; Wang, X. Hybrid Soft Segments Boost the Development of ultratough Thermoplastic Elastomers with Tunable Hardness. *Adv. Mater.* **2025**, *37* (15), No. 2414720.
(40) Huang, Y.; Wu, H.; Li, W.; Yuan, Z.; Wu, Q.; Li, R.; Wu, J. A Healable Poly(Urethane-Urea) Elastomer with Ultra-High Mechanical Strength Enabled by Tailoring Multiple Relaxation Dynamics of Hierarchical Hard Domains. *J. Mater. Chem. A* **2022**, *10* (45), 24290−24300.
(41) Fu, Q.; Li, Y.; Li, W.; Sun, A.; Jing, M.; Liu, X.; Wei, L.; Wu, K. A Self-Reinforcing and Self-Healing Elastomer with High Strength, Unprecedented Toughness and Room-Temperature Reparability. *Mater. Horiz.* **2021**, *8* (1), 267−275.
(42) Lai, Y.; Kuang, X.; Zhu, P.; Huang, M.; Dong, X.; Wang, D. Colorless, Transparent, Robust, and Fast Scratch-Self-Healing Elastomers via a Phase-Locked Dynamic Bonds Design. *Adv. Mater.* **2018**, *30* (38), No. 1802556.
(43) Wang, L.; Zhang, K.; Zhang, X.; Tan, Y.; Guo, L.; Xia, Y.; Wang, X. Mismatched Supramolecular Interactions Facilitate the Reprocessing of Super-Strong and ultratough Thermoset Elastomers. *Adv. Mater.* **2024**, *36* (28), No. 2311758.
(44) Wool, R. P.; O'Connor, K. M. A Theory Crack Healing in Polymers. *J. Appl. Phys.* **1981**, *52* (10), 5953−5963.
(45) Shi, J.; Zheng, T.; Yuan, J.; Qiu, C.; Ha, Y.; Zhang, H.; Guo, B.; Xu, J. Designing a Self-Healing Shape Memory Polymer with High Stiffness and Toughness: The Role of Nonuniform Chain Networks. *Macromolecules* **2024**, *57* (23), 10987−10995.

https://doi.org/10.1021/acsami.5c24286
ACS Appl. Mater. Interfaces 2026, 18, 7452−7461